J Eng Math (2009) 63:309–326
DOI 10.1007/s10665-008-9228-0

A multi-scale approach to the propagation of non-adiabatic premixed flames

Moshe Matalon · John K. Bechtold

Received: 25 May 2007 / Accepted: 17 March 2008 / Published online: 5 April 2008

Abstract Flame propagation involves physico-chemical processes that occur over a range of temporal and spatial scales. By use of a multi-scale analysis it is shown that diffusion processes occurring on relatively small scales can be resolved analytically when the overall activation energy of the chemical reactions is large, thus providing, by asymptotic matching, explicit conditions for the state of the gas and for the flow field across the flame zone. The mathematical formulation on the larger hydrodynamic scale reduces to a free-boundary problem, with the free surface being the flame front. The front propagates into the fresh unburned gas at a rate that depends on both the local strain that it experiences and the local curvature, with coefficients that depend on the diffusion rates of heat and mass, the equivalence ratio of the mixture and the chemical kinetic parameters. The simplified model, properly termed a *hydrodynamic model*, involves the solution of the Navier Stokes equations with different densities and viscosities for the burned and unburned gas. The present work extends earlier studies by including volumetric heat loss, such as radiative loss, which affects the dynamics and may lead to flame extinction.

Keywords Flame extinction · Hydrodynamic theory of flame propagation · Matched asymptotic expansions · Nonadiabatic flames

1 Introduction

Combustion systems involve intricate coupling of gasdynamics, heat and mass transport and chemical reaction rates that occur over a range of temporal and spatial scales. It is not surprising then that the techniques of asymptotic analysis are the primary tools used to systematically derive mathematical models of flame propagation. A model that has contributed a great deal to the theoretical understanding of flame propagation is the hydrodynamic model, which considers the flame to be thin relative to all the other length scales in the problem. As such, the flame front can be regarded as a surface of density discontinuity that separates burned from unburned gases. The full set of governing equations then simplifies to having to solve a free-boundary problem, with the flow on either side determined by the

M. Matalon (✉)
Mechanical Science and Engineering, University of Illinois at Urbana-Champaign, 1206 West Green Street, MC-244, Urbana, IL 61801, USA
e-mail: matalon@uiuc.edu

J. K. Bechtold
Department of Mathematical Sciences, New Jersey Institute of Technology, Newark, NJ 07102, USA

equations of hydrodynamics. The hydrodynamic model dates back to Darrieus [1] and Landau [2] who addressed the linear stability of a planar flame front. They solved the Euler equations on either side of the perturbed flame surface, and related the solutions on each side by imposing conditions of mass and momentum conservation across the front. To complete their formulation, they assumed that the free boundary propagates at a constant speed relative to the underlying flow immediately ahead of the flame surface. These early theories predicted that a planar flame is unconditionally unstable, with wrinkles of short wavelength growing faster than wrinkles of long wavelength. The instability results from thermal expansion which causes an expansion/contraction in streamtubes upon crossing segments of the flame that are concave/convex towards the fresh mixture, respectively. Consequently, a pressure gradient, or equivalently vorticity is generated such as to cause an intrusion in the unburned gas to further increase. The Darrieus–Landau model ignores the flame structure and thus fails to properly describe the behavior of the short wavelength disturbances that are comparable to the flame thickness. An improved model was suggested by Markstein [3, Sect. C.1.4] nearly 20 years later in order to reconcile between the theoretical prediction and the experimental observation of small-scale laboratory planar flames. A linear dependence of the flame speed on curvature was hypothesized leading to stabilization of the short wavelength disturbance when the proportionality constant admits the proper sign. Nevertheless the Darrieus–Landau or hydrodynamic instability is *always* present in flames and, moreover, is dominant in large scale flames where the effects of diffusion, relevant on a scale comparable to the flame thickness, are minimal.

In recent years, it has been recognized that the problem of premixed flame propagation is a singular perturbation problem, in which the internal flame structure evolves on a diffusion length scale, much smaller than the outer hydrodynamic length. Furthermore, chemical reaction is confined to a yet thinner layer embedded in the flame zone, thus forming a nested boundary layer. The methods of boundary-layer analysis have therefore been employed to accurately resolve the inner flame structure. The process of asymptotic matching then provides expressions relating the flow field on either side, as well as an equation describing the evolution of the free boundary—the flame front. Although the first publications describing such models were concerned with systematically re-examining the linear stability of a planar flame front [4–6], it has been since recognized that the general formulation of flames as hydrodynamic discontinuities [5] and its generalization [7–9] have numerous other applications. The formal derivations of hydrodynamic models demonstrate that, to a first approximation, mass and momentum are indeed conserved across the flame and the front propagates at a constant rate relative to the local unburned gas, as originally postulated by Darrieus and Landau. Furthermore, the asymptotic models provide corrections to these conditions, on the order of the flame thickness, that account for accumulation of mass and momentum inside of, and transverse mass and momentum fluxes through, the flame zone. The flame speed too is found to have a linear dependence on stretch, the combined effects of curvature and hydrodynamic strain. The sensitivity of this dependence is given in terms of a coefficient which has become known as the Markstein number [8]; it exhibits an explicit dependence on fundamental flame parameters, such as Lewis number, thermal expansion, activation energy, reaction order and equivalence ratio.

Not included in the aforementioned theories is the effect of volumetric heat loss, such as radiative loss, which can have a significant impact on flame front evolution. Most theories of non-adiabatic flame propagation are either limited to a one-dimensional configuration or formulated within the context of diffusional–thermal theories [10, pp. 118–123], 11–12, [13, Sect. 8.2.1], where thermal-expansion effects have been completely neglected. Exceptions are the stability analysis of a planar flame propagating downward in a tube [14] and the study of self-extinguishing spherically expanding flames [15]. In the present work we present details of an asymptotic analysis, and derive a general theory of *non-adiabatic* premixed flame propagation. The formulation is valid for flames of arbitrary shape propagating in general fluid flows, whether laminar or turbulent. To provide greater quantitative accuracy, we allow for a range of mixture compositions varying from lean to rich. And to better represent a wide range of experimental conditions, we allow for arbitrary reaction orders as well as an arbitrary temperature dependence of the transport coefficients. The results are contrasted with those obtained previously for adiabatic flames. To illustrate the importance of heat loss we also examine the effect of radiative loss in Bunsen flames which is, as we show, partially responsible for the observed phenomenon of tip opening.

2 Governing equations

We consider a premixed flame propagating through a combustible mixture consisting of deficient, and excess reactants, both appearing in relatively small quantities relative to an abundant inert. The chemical reaction proceeds according to

$$\nu_D \mathcal{M}_D + \nu_E \mathcal{M}_E \rightarrow \text{Products}, \tag{1}$$

where $\mathcal{M}_i$ represents the chemical symbol and ν_i the stoichiometric coefficient of species i, with the index $i = D, E$ identifying the deficient/excess reactant, respectively. Typically, one of the $\mathcal{M}_i$ corresponds to a fuel and the other to an oxidizer, and the global reaction (1) models the complex and multi-step oxidation mechanism occurring in practice. The reaction rate is assumed to be proportional to the reactant concentrations $\tilde{\rho} Y_i / W_i$ raised to the powers a and b, respectively; here $\tilde{\rho}$ is the mixture density, Y_i, W_i are the mass fraction and molecular weight of species i and the coefficients a, b, known as the reaction orders, are empirical numbers that mimic the global rate of the complex reaction network. The temperature dependence of the reaction rate obeys an Arrhenius law with an overall activation energy E_a and a pre-exponential factor $\mathcal{B}$. A full nomenclature list is given in the appendix.

We allow for arbitrary mixture compositions ranging from lean to rich conditions. It is thus convenient to introduce the ratio of the mass of excess-to-deficient reactants as $\Phi = Y_{E_\mathrm{u}} / \nu Y_{D_\mathrm{u}}$ where $\nu = \nu_E W_E / \nu_D W_D$ is the mass-weighted stoichiometric coefficient ratio, and the subscript $_\mathrm{u}$ denotes conditions in the unburned state. Note that Φ, as defined, is always larger than unity with $\Phi = 1$ corresponding to a stoichiometric mixture. In the combustion literature it is customary to define the "equivalence ratio" as the ratio of the mass of fuel-to-oxidizer normalized by their stoichiometric proportions. Hence Φ is equal to the equivalence ratio for fuel-rich mixtures and its reciprocal for fuel-lean mixtures.

Deflagrative combustion phenomena are highly subsonic and, as such, a quasi-isobaric limit, yielding a low-Mach-number approximation, is employed in their description. The governing equations are therefore the Navier–Stokes equations for a variable-density gas, assumed to be Newtonian with zero bulk viscosity, supplemented by mass balance equations for the two reactants and an energy equation for the mixture. Consistent with this approximation viscous heating and pressure work, which normally appear in the energy equation, are neglected and the idealized equation of state yields that the density is inversely proportional to the temperature. Since, in the present study, we investigate the interaction between flame and flow under *non-adiabatic* conditions, we also account for volumetric heat losses. We denote by $\tilde{\mathcal{Q}}_\mathrm{L}(\tilde{T})$ the heat-loss rate per unit volume (per unit time) which, in general, is a function of temperature such that $\tilde{\mathcal{Q}}_\mathrm{L} \rightarrow 0$ as $\tilde{T} \rightarrow \tilde{T}_\mathrm{u}$. In gaseous flames, for example, volumetric heat losses are often associated with thermal radiation from soot particles or intermediate products generated during combustion. In this case, the energy-loss term can be expressed in the optically thin limit, as

$$\tilde{\mathcal{Q}}_\mathrm{L} = 4\hat{\sigma} l_p^{-1} \left(\tilde{T}^4 - \tilde{T}_\mathrm{u}^4 \right),$$

where $\tilde{T}_\mathrm{u}$ is the ambient temperature, $\hat{\sigma}$ the Stefan-Boltzmann constant and l_p the Planck mean absorption length.

The notation adopted in this paper is to use the same variables for both dimensional and dimensionless quantities, with the understanding that a '~' on top of the variable identifies it as the dimensional quantity.

We non-dimensionalize lengths with the hydrodynamic length scale, L, which characterizes the size of the flame, or the size of the vessel within which the flame propagates, and velocities with respect to the (adiabatic) laminar flame speed, S_L. An appropriate time scale is then L/S_L. Diffusion introduces another length scale $L_\mathrm{D} = \mathcal{D}_{th}/S_\mathrm{L}$, where $\mathcal{D}_{th}$ is the thermal diffusivity of the mixture, so that $\delta \equiv L_\mathrm{D}/L$. The density of the mixture is scaled with respect to its value in the fresh mixture $\tilde{\rho}_\mathrm{u}$, and the pressure is scaled using $\tilde{\rho}_\mathrm{u} S_\mathrm{L}^2$. The specific heats of all species are assumed equal, and equal to a constant value c_p. The viscosity $\tilde{\mu}$, thermal conductivity $\tilde{\lambda}$ and molecular diffusivity $\tilde{D}_i$ (binary diffusivity of reactant–inert) are assumed to depend on temperature $\tilde{T}$, and they are scaled with respect to their values in the fresh mixture, namely at a state where $\tilde{T} = \tilde{T}_\mathrm{u}$. Although the dependence of transport coefficients on temperature is arbitrary, the ratios consisting of the Prandtl number $\mathrm{Pr} = \tilde{\mu} c_p / \tilde{\lambda}$ and the Lewis numbers $\mathrm{Le}_i = \tilde{\lambda} / c_p \tilde{\rho} \tilde{D}_i$ are assumed constant, so that

$$\frac{\tilde{\lambda}}{\tilde{\lambda}_{\rm u}} = \frac{\tilde{\rho}\tilde{D}_i}{\tilde{\rho}_{\rm u}\tilde{D}_{i_{\rm u}}} = \frac{\tilde{\mu}}{\tilde{\mu}_{\rm u}} \equiv \lambda,$$

with λ a function of temperature. Let Q be the total heat released during combustion. We choose as a unit of temperature the heat released per unit mass of $\mathcal{M}_D$ supplied, namely $QY_{D_{\rm u}}/(c_p\nu_D W_D)$, which defines the adiabatic flame temperature

$$\tilde{T}_a = \tilde{T}_{\rm u} + QY_{D_{\rm u}}/c_p\nu_D W_D.$$

It is convenient in the following to introduce as a new temperature variable the difference of the local temperature from its value in the fresh mixture, namely $\Theta = (\tilde{T} - \tilde{T}_{\rm u})/(\tilde{T}_a - \tilde{T}_{\rm u})$ Thus, for a planar adiabatic flame that consumes all the available deficient reactant, Θ varies from zero to one. Finally, the heat-loss term is scaled with respect to $\lambda_{\rm u}(\tilde{T}_a - \tilde{T}_{\rm u})/L_{\rm D}^2$.

In dimensionless form the governing equations are

$$\rho\,\{1 + (\sigma - 1)\Theta\} = 1, \quad \frac{\partial\rho}{\partial t} + \boldsymbol{\nabla}\cdot(\rho\mathbf{v}) = 0, \tag{2,3}$$

$$\rho\frac{{\rm D}\mathbf{v}}{{\rm D}t} = -\boldsymbol{\nabla}p + \delta\,{\rm Pr}\;\boldsymbol{\nabla}\cdot\lambda\boldsymbol{\Sigma}, \quad \rho\frac{{\rm D}\Theta}{{\rm D}t} - \delta\boldsymbol{\nabla}\cdot(\lambda\boldsymbol{\nabla}\Theta) = \delta^{-1}(\varpi - Q_{\rm L}), \tag{4,5}$$

$$\rho\frac{{\rm D}Y_D}{{\rm D}t} - \delta{\rm Le}_D^{-1}\boldsymbol{\nabla}\cdot(\lambda\boldsymbol{\nabla}Y_D) = -\delta^{-1}Y_{D_{\rm u}}\varpi, \quad \rho\frac{{\rm D}Y_E}{{\rm D}t} - \delta{\rm Le}_E^{-1}\boldsymbol{\nabla}\cdot(\lambda\boldsymbol{\nabla}Y_E) = -\delta^{-1}\nu Y_{D_{\rm u}}\varpi. \tag{6,7}$$

Here ${\rm D}/{\rm D}t \equiv \partial/\partial t + \mathbf{v}\cdot\boldsymbol{\nabla}$ is the convective derivative with t the time variable, $\mathbf{v}$ is the velocity vector and Σ the viscous stress tensor given by

$$\Sigma = 2\mathbf{E} - \frac{2}{3}(\boldsymbol{\nabla}\cdot\mathbf{v})\mathbf{I}, \qquad \mathbf{E} = \frac{1}{2}\left\{\boldsymbol{\nabla}\mathbf{v} + (\boldsymbol{\nabla}\mathbf{v})^{\rm T}\right\}$$

with $\mathbf{I}$ a unit tensor and the superscript $^{\rm T}$ denoting the transpose. The mass fraction of the inert can be found a posteriori by solving a diffusion equation, similar to (6) or (7), with no source or sink on its right-hand side. And, although an equation for the mass fraction of the products can be written, it is unnecessary because the distribution of product follows immediately from the constraint that all mass fractions sum to unity. The unburned-to-burned density ratio, or thermal expansion parameter, is denoted by $\sigma \equiv \tilde{\rho}_{\rm u}/\tilde{\rho}_{\rm b}$, with the subscript $_{\rm b}$ identifying the state of the burned gas.

The reaction rate ϖ is given by

$$\varpi = \mathcal{D}\,\rho^{a+b}Y_D^a Y_E^b\,\exp\left\{\frac{\beta\sigma(\Theta - 1)}{1 + (\sigma - 1)\Theta}\right\}, \tag{8}$$

where $\beta = E_a(\tilde{T}_a - \tilde{T}_{\rm u})/R^o\tilde{T}_a^2$ is the Zel'dovich number, with R^o the gas constant, and

$$\mathcal{D} = \frac{\tilde{\rho}_{\rm u}^{a+b+1}}{W_D^a W_E^b}\frac{\nu_D W_D}{Y_{D_{\rm u}}}\frac{\mathcal{D}_{th}/S_{\rm L}^2}{(\mathcal{B}{\rm e}^{-E/R^o\tilde{T}_a})^{-1}} \tag{9}$$

is the Damköhler number, the ratio of the flow to the chemical reaction times.

If the following large-activation-energy expression for the adiabatic laminar flame speed,

$$S_{\rm L} = \left\{\frac{2\,\tilde{\rho}_{\rm b}^{\,a+b}(\tilde{\lambda}_{\rm b}/c_p)}{\tilde{\rho}_{\rm u}^2\,\beta^{a+b+1}}\frac{\nu_E^b\,Y_{D_{\rm u}}^{a+b-1}\,\mathcal{G}(a,b;\varphi/{\rm Le}_E)}{\nu_D^{b-1}W_D^{a+b-1}}{\rm Le}_D^a{\rm Le}_E^b\,\mathcal{B}\right\}^{1/2}\exp(-E_a/2R^o\tilde{T}_a) \tag{10}$$

is used in (9), the Damköhler number may be expressed in the form

$$\mathcal{D} = \frac{(\tilde{\rho}_{\rm b}/\tilde{\rho}_{\rm u})^{a+b}\beta^{a+b+1}}{2\,{\rm Le}_D^a\,{\rm Le}_E^b\,\mathcal{G}(a,b;\varphi/{\rm Le}_E)}\frac{\tilde{\lambda}_{\rm u}}{\tilde{\lambda}_{\rm b}}\frac{\Phi^b}{Y_{D_{\rm u}}^a Y_{E_{\rm u}}^b}. \tag{11}$$

The positive coefficient $\mathcal{G}(a, b; \varphi/\mathrm{Le}_E)$, depends on the reaction orders a, b, the excess reactant Lewis number Le_E and the parameter $\varphi \equiv \beta(\Phi - 1)$ that measures the departure from stoichiometry. It is defined in general as

$$\mathcal{G}(a, b; S) \equiv \int_0^\infty \varsigma^a (\varsigma + S)^b \mathrm{e}^{-\varsigma}\, \mathrm{d}\varsigma;$$

when $\varphi = 0$ it can be expressed in terms of the Gamma function, $\mathcal{G} = \Gamma(a+b+1)$, and for $a = b = 1$ it simplifies to $\mathcal{G} = 2+S$. Finally, we note that λ and Q_{L} are both prescribed functions of the temperature $\tilde{T}/\tilde{T}_{\mathrm{u}} = 1+(\sigma-1)\Theta$.

3 The multi-scale approach

The governing equations presented in the previous section can be analyzed through a multi-scale approach, by exploiting the disparity in length scales associated with gasdynamics L, diffusion L_{D}, and chemical reaction $\beta^{-1}L_{\mathrm{D}}$. The ratio $L_{\mathrm{D}}/L = \delta$, is typically much less than unity, often less than 10^{-1}, and the activation energies of the chemical reactions encountered in combustion systems are large compared to the thermal energies of the fresh mixtures, with $\beta \approx 10$.

In the following sections, we will show how these parameters can be systematically exploited to simplify the governing equation (2–8) and derive a new model describing the dynamics of non-adiabatic premixed flames. The flame, consisting of the region where diffusion processes and chemical reaction occur, is a thin layer in the overall flow field that shrinks to a surface as $\delta \to 0$. When viewed on the hydrodynamic length scale, the flame surface separates burned from unburned gases with the flow field on either side governed by the incompressible Euler equations, but with different densities. Viscous effects enter the formulation as a correction term of $\mathcal{O}(\delta)$. The analysis of the internal structure of the flame, which will be presented below, provides the conditions relating the state of the gas and the flow velocities across the flame and determines an explicit relation for the instantaneous shape and location of the flame surface. Although the equations in the flame zone are quasi-steady and quasi-one-dimensional, they contain the highly nonlinear reaction rate term. For large β, however, the chemical activity is highly concentrated within a thin layer where diffusion and chemical reaction dominate. This thin reaction zone, of $\mathcal{O}(\delta\beta^{-1})$, resides inside the flame zone. On the length scale L the reaction sheet and flame front coincide and are represented by a moving free surface $F(\mathbf{x}, t) = 0$. Asymptotic matching of the relevant solutions in each layer explicitly determines the interaction across all scales of the various physical processes involved and, consequently, the instantaneous shape and the jump conditions across that surface.

In the next sections we first discuss the structure of the reaction zone in the limit $\beta \to \infty$ and then analyze the structure of the flame zone by additionally assuming that $\delta \to 0$. Only the essential steps will be presented here; the reader interested in further details should consult the earlier work on adiabatic flames [5,8].

It is convenient for the analysis of the flame structure to introduce a curvilinear coordinate system (n, ξ_1, ξ_2) attached to the moving surface $F = 0$. Here, n is the distance from the reaction sheet in the direction of the unit normal, $\mathbf{n}$, pointing towards the burned gas, and ξ_1, ξ_2 are intrinsic surface coordinates aligned with the principal directions of curvature at each point of the surface. The velocity of the front, back along its normal, as measured from a fixed coordinate system is $V_f = -\partial n/\partial t$, or equivalently $V_f = -F_t/|\nabla F|$. If $\mathbf{e_1}, \mathbf{e_2}$ denote the unit vectors tangential to the parametric curves $\xi_2 = \text{const}$ and $\xi_1 = \text{const}$, respectively, the vectors $\mathbf{n}, \mathbf{e}_1, \mathbf{e}_2$ form an orthogonal triad of unit vectors. The transformation to the new coordinate system requires expressing the various vector operators as well as the time derivative in the moving intrinsic frame.[1]

4 The reaction zone

For $\beta \gg 1$ the reaction rate (8) is exponentially small except when $\Theta - 1 = \mathcal{O}(\beta^{-1})$, namely in the reaction zone, where the temperature is near the adiabatic flame temperature. To ensure that temperature and concentration

[1] Vector operators in curvilinear coordinates attached to a fixed surface can be found in textbooks on differential geometry; the transformation to curvilinear coordinates attached to a *moving* surface has been derived in [8].

gradients remain finite, the thickness of this region must scale as $\mathcal{O}(\beta^{-1})$. Self-consistency of the asymptotic treatment also requires a near-equidiffusion formulation [16] whereby $\mathrm{Le}_i^{-1} = 1 - \beta^{-1}\,\mathrm{le}_i$, a near-stoichiometric mixture limit [8] for which $Y_{E_\mathrm{u}} - \nu Y_{D_\mathrm{u}} = \mathcal{O}(\beta^{-1})$, namely $\varphi = \beta(\Phi - 1) = \mathcal{O}(1)$, and a small heat-loss term such that $Q_\mathrm{L} = k\beta^{-1}g(T)$ where k is a heat-transfer coefficient and g a function of temperature $T = 1 + (\sigma - 1)\Theta$. For radiative loss, for example, $k = 4\beta L_D^2 \hat{\sigma} l_p^{-1} \tilde{T}_\mathrm{u}^4/\lambda_\mathrm{u}(\tilde{T}_a - \tilde{T}_\mathrm{u})$ and $g(T) = T^4 - 1$.

It is convenient to introduce the enthalpy functions, h_D and h_E, defined from the relations

$$\Theta + \frac{Y_D}{Y_{D_\mathrm{u}}} = 1 + \beta^{-1}h_D + \cdots, \qquad \Theta + \frac{Y_E}{Y_{E_\mathrm{u}}} = 1 + \beta^{-1}h_E + \cdots$$

along with the expansion $\Theta = \theta + \beta^{-1}\theta_1 + \cdots$ (we have avoided the subscript $_0$ in the leading term to simplify the notation). Since outside the reaction zone $\varpi \sim 0$, the relevant governing equations, to leading order, reduce to

$$\rho\frac{\mathrm{D}\theta}{\mathrm{D}t} - \delta\boldsymbol{\nabla}\cdot(\lambda\boldsymbol{\nabla}\theta) = 0, \quad \rho\frac{\mathrm{D}h_i}{\mathrm{D}t} - \delta\boldsymbol{\nabla}\cdot(\lambda\boldsymbol{\nabla}h_i) = \delta\mathrm{le}_i\,\boldsymbol{\nabla}\cdot(\lambda\boldsymbol{\nabla}\theta) - \delta^{-1}kg. \tag{12,13}$$

To analyze the reaction zone, we introduce the stretching transformation $n = \hat{\eta}/\beta$ and the inner expansions

$$\Theta = 1 + \beta^{-1}\hat{\theta} + \cdots, \quad h_i = h_i^* + \cdots,$$

where the superscript $*$ implies evaluation at $n = 0^+$ so that $h_i^* = h_i^*(\xi_1, \xi_2, t)$. Substituting in the appropriate governing equations, one finds

$$-\lambda_\mathrm{b}\delta^2\frac{\partial^2\hat{\theta}}{\partial\hat{\eta}^2} = \Lambda(h_D^* - \hat{\theta})^a(h_E^* - \hat{\theta})^b\,\mathrm{e}^{\hat{\theta}},$$

where $\Lambda = \beta^{-1}\nu^b\mathrm{Le}_D^a\mathrm{Le}_E^b(Y_{D_\mathrm{u}}/\beta\sigma)^{a+b}\,\mathcal{D}$. Multiplying by $\partial\hat{\theta}/\partial\hat{\eta}$ and integrating across the reaction zone one finds

$$-\frac{1}{2}\lambda_\mathrm{b}\delta^2\left(\frac{\partial\hat{\theta}}{\partial\hat{\eta}}\right)^2\Bigg|_{-\infty}^{\infty} = \Lambda\int_{-\infty}^{\theta^*}(h_D^* - \hat{\theta})^a(h_E^* - \hat{\theta})^b\,\mathrm{e}^{\hat{\theta}}\,\mathrm{d}\hat{\theta}.$$

Matching as $\hat{\eta} \to -\infty$ yields

$$\lambda_\mathrm{b}\delta^2\left(\frac{\partial\theta}{\partial n}\right)^2\Bigg|_{n=0^-} = 2\Lambda\,\mathrm{e}^{\theta_1^*}\int_0^{\infty}(h_D^* - \theta_1^* + z)^a(h_E^* - \theta_1^* + z)^b\,\mathrm{e}^{-z}\,\mathrm{d}z, \tag{14}$$

where use has been made of the requirement $\hat{\theta} \sim \theta_1^*(\xi_1, \xi_2, t)$ as $\hat{\eta} \to \infty$. Note that the flame temperature perturbation θ_1^* assumes the values h_D^* or h_E^*, depending on whether $\mathcal{M}_D$ or $\mathcal{M}_E$ is depleted in the reaction zone, respectively, and the difference $\left|h_E^* - h_D^*\right|$ represents the extent of the unconsumed reactant that leaks through. Finally, when substituting for Λ, the right-hand side of (14) simplifies to $\mathrm{e}^{\theta_1^*}\,\mathcal{G}(a, b; \left|h_E^* - h_D^*\right|)/\mathcal{G}(a, b; \varphi/Le_E)$.

Since Eq. 13 and the remaining fluid equations do not contain source terms, a straightforward integration across the reaction zone yields, after matching, jump relationships across $n = 0$. The results are summarized below

$$[\theta] = [h_i] = 0, \quad \left[\lambda\frac{\partial h_i}{\partial n}\right] = -\,\mathrm{le}_i\left[\lambda\frac{\partial\theta}{\partial n}\right], \tag{15}$$

$$\delta\left[\lambda\frac{\partial\theta}{\partial n}\right] = -\left\{\frac{\mathcal{G}(a, b; |\,h_E^* - h_D^*|)}{\mathcal{G}(a, b;\,\varphi)}\right\}^{1/2}\exp(\theta_1^*/2), \tag{16}$$

$$[\mathbf{v}] = 0, \quad [p] = \frac{4}{3}\,\mathrm{Pr}\left[\lambda\frac{\partial}{\partial n}(\mathbf{v}\cdot\mathbf{n})\right], \tag{17}$$

$$\left[\frac{\partial}{\partial n}\rho(\mathbf{v}\cdot\mathbf{n} - V_f)\right] = 0, \quad \left[\frac{\partial}{\partial n}\,(\mathbf{n}\times(\mathbf{v}\times\mathbf{n}))\right] = 0, \tag{18}$$

where $[\cdot]$ denotes the jump in the quantity, specifically the value at the burned side minus that on the unburned side of the sheet.

5 The flame zone

We now consider the limit $\delta \ll 1$. Since, to leading order, the diffusion terms are negligible, except in the thin flame surrounding the reaction sheet, the transport equations in the outer zones reduce to $\mathrm{D}\theta/\mathrm{D}t = \mathrm{D}h_i/\mathrm{D}t = 0$. The state of the fresh mixture, therefore, remains uniform and given by

$$\theta = 0,\ Y_D = Y_{D_\mathrm{u}},\ Y_E = Y_{E_\mathrm{u}} \quad \text{for } F < 0, \tag{19}$$

where $F = 0$ represents the flame front. Consistent with the previous assumptions the temperature and reactant concentrations in the burned gas are

$$\theta = 1 + \mathcal{O}(\beta^{-1}),\ Y_D = 0,\ Y_E = Y_{E_\mathrm{u}}(\Phi - 1) + \mathcal{O}(\beta^{-1}) \quad \text{for } F > 0. \tag{20}$$

It is assumed here that $\mathcal{M}_D$ is the reactant depleted at the reaction sheet, which is always the case when $\varphi = \mathcal{O}(1)$ as will be verified below. The enthalpies in the burned region are therefore given by $h_D = 0$ and $h_E = \varphi$. We remark that by re-scaling $\varphi = \mathcal{O}(\delta)$, it is possible for the initially excess reactant to be locally deficient near the reaction sheet, and hence consumed, while the initially deficient reactant leaks through. This case differs from the one presented here in some minor mathematical detail, which we do not bother to pursue. A discussion of the various scenarios that can take place under near-stoichiometric conditions can be found in [17,18]. Similar to heat and mass, viscous diffusion in the outer zones is negligible to leading order, and the flow field is consequently described by Euler's equations but with a piecewise-constant density $\rho = 1$ on the unburned side, and $\rho = 1/\sigma$ (corresponding to $\theta = 1$) on the burned side. Viscous effects are incorporated as $\mathcal{O}(\delta)$ perturbations, with the viscosity given by $\lambda = 1$ on the unburned side, and $\lambda = \lambda_\mathrm{b}$ on the burned side. The downstream region consists of a near field, on the hydrodynamic length scale, with a nearly uniform temperature distribution, and an $\mathcal{O}(\beta)$ far field where the temperature decays to its equilibrium value due to losses. However, the far field does not influence the flame front dynamics, and so details of its analysis will not be presented here.

It is convenient in the following analysis to decompose the velocity vector into components normal and tangential to the surface using the notation $\mathbf{v} = \mathbf{v}_\perp + v_n\,\mathbf{n}$. We will use lower case letters $(v_n, \mathbf{v}_\perp)$ to denote solutions in the flame zone, and upper case letters $(V_n, \mathbf{V}_\perp)$ to denote solutions the outer hydrodynamic regions. We also introduce the mass flux in the normal direction to the front, $m \equiv \rho(v_n - V_f)$, as a new variable which, when evaluated just ahead of the flame at $n = 0^-$, represents the mass burning rate. The *flame speed*, S_f, is conventionally defined as the velocity of the flame front relative to the unburned gas, so that $S_f = V_n|_{n=0^-} - V_f$.

To examine the structure of the flame zone, we introduce the stretching transformation

$$\eta = \int_0^{n/\delta} \frac{1}{\lambda}\,\mathrm{d}n', \tag{21}$$

and expand all variables in power series of δ, namely of the form $V_n = v_{n_0} + \delta v_{n_1} + \cdots$. The solution must satisfy the jump[2] conditions (15), (18) across $\eta = 0$ and must be matched as $\eta \to \pm\infty$ with the outer variables. The state variables are readily matched to the unburned and burned states given by (19–20), respectively. For the matching purpose, the outer solutions for the pressure and velocities must be expanded in Taylor series about $n = 0^\pm$. Using the transformation (21) the matching conditions take the form

$$v_n \sim V_{n_0}\big|_{n=0^\pm} + \delta\left\{\left.\frac{\partial V_{n_0}}{\partial n}\right|_{n=0^\pm}\int_0^\eta \lambda\,\mathrm{d}\eta' + V_{n_1}\big|_{n=0^\pm}\right\}.$$

The leading order governing equations are

$$\frac{\partial m_0}{\partial \eta} = 0, \quad m_0\frac{\partial \theta_0}{\partial \eta} - \frac{\partial^2\theta_0}{\partial \eta^2} = 0, \quad m_0\frac{\partial h_{i_0}}{\partial \eta} - \frac{\partial^2 h_{i_0}}{\partial \eta^2} = \mathrm{le}_i\frac{\partial^2\theta_0}{\partial \eta^2} - k\lambda(\tau)\,g(\tau),$$

$$m_0\frac{\partial v_{n_0}}{\partial \eta} - \frac{4}{3}\mathrm{Pr}\,\frac{\partial^2 v_{n_0}}{\partial \eta^2} = -\frac{\partial p_0}{\partial \eta}, \quad m_0\frac{\partial \mathbf{v}_{\perp_0}}{\partial \eta} - \mathrm{Pr}\,\frac{\partial^2 \mathbf{v}_{\perp_0}}{\partial \eta^2} = 0,$$

[2] Note that according to the stretching transformation (21), we have $\lambda\delta\,\partial/\partial n = \partial/\partial\eta$, so that all derivatives in these relations are replaced by $\partial/\partial\eta$.

where $\tau \equiv 1 + (\sigma - 1)\theta_0$, so that the last term on the right-hand side of (5) is an implicit function of η. Solutions that satisfy the jump relations at $\eta = 0$ and the matching conditions as $\eta \to -\infty$, are found to be

$$\theta_0 = \begin{cases} \mathrm{e}^{m_0\eta} \\ 1 \end{cases}, \quad \rho_0 = \begin{cases} \{1 + (\sigma - 1)\,\mathrm{e}^{m_0\eta}\}^{-1} \\ \sigma^{-1} \end{cases},$$

$$h_{D_0} = \begin{cases} -\mathrm{le}_D\, m_0\eta\, \mathrm{e}^{m_0\eta} + \dfrac{k}{m_0^2}\,(\chi_1(\eta) - q_\mathrm{u} - q_\mathrm{b}\mathrm{e}^{m_0\eta}) \\ -\dfrac{k}{m_0^2}\,((\eta+1)q_\mathrm{b} + q_\mathrm{u}) \end{cases},$$

$$h_{E_0} = \begin{cases} \varphi - \mathrm{le}_E\, m_0\eta\, \mathrm{e}^{m_0\eta} + \dfrac{k}{m_0^2}\,(\chi_1(\eta) - q_\mathrm{u} - q_\mathrm{b}\mathrm{e}^{m_0\eta}) \\ \varphi - \dfrac{k}{m_0^2}\,((\eta+1)q_\mathrm{b} + q_\mathrm{u}) \end{cases},$$

$$p_0 = P_0|_{n=0^-} + \begin{cases} \left(\dfrac{4}{3}\mathrm{Pr} - 1\right)(\sigma - 1)m_0^2\,\mathrm{e}^{m_0\eta} \\ -(\sigma - 1)m_0^2 \end{cases},$$

$$v_{n_0} = V_{n_0}\big|_{n=0^-} + \begin{cases} (\sigma - 1)m_0\,\mathrm{e}^{m_0\eta} \\ (\sigma - 1)m_0 \end{cases}, \quad \mathbf{v}_{\perp_0} = \mathbf{V}_{\perp_0}\big|_{n=0^-},$$

where

$$\chi_1(\eta) = \int_{\tau(\eta)}^{\sigma} \frac{x - \tau(\eta)}{(x-1)^2}\,\lambda(x)g(x)\,\mathrm{d}x.$$

Matching on both sides of the flame zone also provides jump relations

$$[\![V_{n_0}]\!] = (\sigma - 1), \qquad [\![\mathbf{V}_{\perp_0}]\!] = 0, \qquad [\![P_0]\!] = -(\sigma - 1)m_0^2, \tag{22}$$

where $[\![\cdot]\!] = (\cdot)_{n=0^+} - (\cdot)_{n=0^-}$ denotes the jump across the flame zone, and an expression for the mass burning rate in the form

$$m_0^2\,\log m_0^2 = -k(q_\mathrm{u} + q_\mathrm{b}), \tag{23}$$

where the constants

$$q_\mathrm{u} = \int_1^{\sigma} \frac{\lambda(x)\,g(x)}{x-1}\mathrm{d}x, \quad q_\mathrm{b} = \lambda_\mathrm{b}\,g(\sigma)$$

represent the integrated losses from the unburned and burned gas regions, respectively. Equation (23) implies that, to leading order, the flame speed is given by

$$S_{f_0} = V_{n_0}\big|_{n=0^-} - V_{f_0} = m_0. \tag{24}$$

Thus, to a first approximation, the flame speed of a curved flame is equal to the speed of a planar flame with the same intensity of heat loss. In the absence of heat losses it is equal to the adiabatic flame speed, with $S_{f_0} = 1$.

To assess the role of the processes that are dominant in the flame zone, we proceed to the next order in the perturbation scheme. To $\mathcal{O}(\delta)$ we have

$$\frac{1}{\lambda}\frac{\partial m_1}{\partial \eta} = m_0\kappa - \rho_0\mathbb{K}, \quad m_0\frac{\partial \theta_1}{\partial \eta} - \frac{\partial^2\theta_1}{\partial\eta^2} = -(m_1 + \lambda\kappa)\frac{\partial\theta_0}{\partial\eta}, \tag{25,26}$$

$$m_0\frac{\partial h_{i_1}}{\partial\eta} - \frac{\partial^2 h_{i_1}}{\partial\eta^2} = -(m_1 + \lambda\kappa)\frac{\partial h_{i_0}}{\partial\eta} + \mathrm{le}_i\frac{\partial^2\theta_1}{\partial\eta^2} - \lambda\mathrm{le}_i\,\kappa\frac{\partial\theta_0}{\partial\eta} - k(\sigma-1)\theta_1\frac{\mathrm{d}(\lambda g)}{\mathrm{d}\tau}. \tag{27}$$

Here $\mathbb{K}$ is the combination of curvature and hydrodynamic strain, known as *flame stretch* [19]. It is a measure of the flame-surface deformation that results from its motion and the variations in the underlying flow field. A general invariant expression for stretch is given by $\mathbb{K} = S_f\,\kappa + \mathbb{K}_s$ where $\kappa = -\nabla\cdot\mathbf{n}$ is the local curvature and $\mathbb{K}_s = -\mathbf{n}\cdot\mathbf{E}\cdot\mathbf{n}$ the local strain rate (see also Appendix A in [8]). Note that in the present context $\mathbb{K} \sim m_0\kappa + \mathbb{K}_s$.

Equation (25) can be integrated to give

$$m_1 = f_1 + \begin{cases} \kappa\, I(\eta) - m_0^{-1}\,\mathbb{K}\, J(\eta) \\ \lambda_\mathrm{b}(m_0\kappa\ - \sigma^{-1}\mathbb{K})\,\eta \end{cases}, \tag{28}$$

where

$$I(\eta) = m_0\int_0^\eta \lambda \mathrm{d}\eta = -\int_\tau^\sigma \frac{\lambda(x)}{x-1}\,\mathrm{d}x, \quad J(\eta) = m_0\int_0^\eta \rho_0\lambda \mathrm{d}\eta = -\int_\tau^\sigma \frac{\lambda(x)}{x(x-1)}\,\mathrm{d}x,$$

and $f_1 = f_1(\xi_1, \xi_2, t)$ remains to be determined. This is achieved by solving for θ_1 and h_{i_1} and applying the jump relations across the reaction sheet, as follows.

In the burned region $\theta_1 = 0$, so that when integrating (26) for $\eta < 0$ using the appropriate matching and jump conditions one finds

$$\theta_1 = f_1\,\eta \mathrm{e}^{m_0\eta} + \chi_2(\eta) + \frac{\gamma_1\mathbb{K}}{\sigma m_0^2}\left(\mathrm{e}^{m_0\eta} - 1\right), \tag{29}$$

where

$$\chi_2(\eta) = \int_\eta^0 \left(\kappa\, I(\eta') - \frac{\mathbb{K}}{m_0}J(\eta') + \lambda\kappa\right)\left(\mathrm{e}^{m_0\eta'} - \mathrm{e}^{m_0\eta}\right)\mathrm{d}\eta', \quad \gamma_1 = \frac{\sigma}{\sigma-1}\int_1^\sigma \frac{\lambda(x)}{x}\,\mathrm{d}x.$$

The jump in the gradient of θ_1 across the reaction sheet $\eta = 0$ can now be easily evaluated.

Next we need to compute the jump in the gradients of h_{i_1} across the reaction sheet. We first consider the enthalpy equations (27) in the burned region ($\eta > 0$)

$$m_0\frac{\partial h_{i_1}}{\partial\eta} - \frac{\partial^2 h_{i_1}}{\partial\eta^2} = \frac{kq_\mathrm{b}}{m_0}\left\{\left(m_0\kappa - \frac{\mathbb{K}}{\sigma}\right)\lambda_\mathrm{b}\eta + f_1 + \lambda_\mathrm{b}\kappa\right\}.$$

These equations are integrated to give

$$h_{i_1} = h_{i_1}^* + \frac{kq_\mathrm{b}}{m_0^2}\left\{\left(f_1 + 2\lambda_\mathrm{b}\kappa - \frac{\lambda_\mathrm{b}\mathbb{K}}{\sigma m_0}\right)\eta + \frac{1}{2}\lambda_\mathrm{b}\left(m_0\kappa - \frac{\mathbb{K}}{\sigma}\right)\eta^2\right\},$$

from which the gradients $\partial h_{i_1}/\partial\eta$ at $\eta = 0^+$ are readily available. We recall that the superscript * indicates the common value at $\eta = 0^\pm$. Since h_{i_1} and their gradients vanish as $\eta \to -\infty$, all that is needed is an integration of (27) across the entire unburned gas region, i.e. from $\eta = -\infty$ to $\eta = 0^-$. One finds

$$\begin{aligned} m_0 h_{i_1}\Big|_{-\infty}^{0^-} - \frac{\partial h_{i_1}}{\partial\eta}\Big|_{-\infty}^{0^-} &= \int_{-\infty}^{0^-}\left(\kappa I - m_0^{-1}\mathbb{K}J + \lambda\kappa + f_1\right)\left\{\mathrm{le}_i\, m_0(1+m_0\eta)\mathrm{e}^{m_0\eta} - \frac{k}{m_0^2}\frac{\mathrm{d}\chi_1}{\mathrm{d}\eta} + \frac{kq_\mathrm{b}}{m_0}\mathrm{e}^{m_0\eta}\right\}\mathrm{d}\eta \\ &\quad + \mathrm{le}_i\,\frac{\partial\theta_1}{\partial\eta}\Big|_{-\infty}^{0^-} - \mathrm{le}_i\,\kappa\int_{-\infty}^{0^-}\lambda m_0\mathrm{e}^{m_0\eta}\mathrm{d}\eta - k(\sigma-1)\int_{-\infty}^{0^-}\theta_1\frac{\mathrm{d}(\lambda g)}{\mathrm{d}\tau}\mathrm{d}\eta, \end{aligned}$$

from which the gradients $\partial h_{i_1}/\partial\eta$ at $\eta = 0^-$ can be evaluated. Note that the last term, which contains all the effects of heat loss, can be simplified to

$$k(\sigma-1)\int_{-\infty}^{0^-}\frac{\mathrm{d}(\lambda g)}{\mathrm{d}\eta}\frac{\mathrm{d}\eta}{\mathrm{d}\tau}\theta_1\mathrm{d}\eta = \frac{k}{m_0}\int_{-\infty}^{0^-}\frac{\mathrm{d}(\lambda g)}{\mathrm{d}\eta}\theta_1\mathrm{e}^{-m_0\eta}\mathrm{d}\eta$$

and, after repeated use of integration by parts, one obtains

$$k(\sigma-1)\int_{-\infty}^{0^-}\theta_1\frac{\mathrm{d}(\lambda g)}{\mathrm{d}\tau}\mathrm{d}\eta = \frac{1}{m_0^2}\left((s_1+s_3)\kappa - \frac{s_2}{m_0}\mathbb{K} - q_\mathrm{u}f_1\right),$$

where

$$s_1 = \int_1^\sigma \left(\int_y^\sigma \frac{\lambda(x)}{x-1} \mathrm{d}x \right) \left(\int_y^\sigma \frac{\lambda(x) g(x)}{(x-1)^2} \mathrm{d}x \right) \mathrm{d}y, \quad s_2 = \int_1^\sigma \left(\int_y^\sigma \frac{\lambda(x)}{x(x-1)} \mathrm{d}x \right) \left(\int_y^\sigma \frac{\lambda(x) g(x)}{(x-1)^2} \mathrm{d}x \right) \mathrm{d}y,$$

$$s_3 = -\int_1^\sigma \lambda(y) \int_y^\sigma \frac{\lambda(x) g(x)}{(x-1)^2} \mathrm{d}x \, \mathrm{d}y.$$

With the jump in the gradients of h_{i_1} known across the reaction sheet, the condition (15) can now be satisfied. This yields

$$h_{i_1}^* = -\frac{\gamma_2 \mathbb{K}}{m_0^2} \mathrm{le}_i + \frac{2k}{m_0^3} (q_\mathrm{u} + q_\mathrm{b}) f_1 + \frac{k}{m_0^3} B, \quad B = \left(\frac{q_\mathrm{b}}{\sigma} (\gamma_1 - \lambda_\mathrm{b}) + 2 s_2 \right) \frac{\mathbb{K}}{m_0} + 2 \left(\lambda_\mathrm{b} q_\mathrm{b} - s_1 - s_3 \right) \kappa,$$

where

$$\gamma_2 = \frac{1}{\sigma - 1} \int_1^\sigma \frac{\lambda(x)}{x} \log \left(\frac{\sigma - 1}{x - 1} \right) \mathrm{d}x.$$

We note that the local concentration difference between the excess and deficient reactants at the reaction sheet is proportional to the difference in enthalpies

$$h_E^* - h_D^* = \varphi - \delta (\gamma_2 / m_0^2) (\mathrm{le}_E - \mathrm{le}_D) \mathbb{K}, \tag{30}$$

which is always positive when $\varphi = \mathcal{O}(1)$. This implies that the deficient reactant in the fresh mixture is the one depleted in the reaction zone, as assumed earlier. Consequently, $\theta_1^* = h_D^*$ and the relation (30) is used to determine the extent of the reactant $\mathcal{M}_E$ that leaks through the sheet. Now the condition (16) can be also satisfied providing an expression for f_1,

$$f_1 = \frac{(-\alpha + \gamma_1 (\sigma - 1)/\sigma) \, m_0 \mathbb{K} + \frac{1}{2} k B}{m_0^2 - k \, (q_\mathrm{u} + q_\mathrm{b})},$$

which completely determines the mass flux m_1 (see Eq. 28). Note that, with m_0 given by (23), the denominator is positive definite and consequently m_1 is always well defined. The coefficient α here is given by

$$\alpha = \gamma_1 + \frac{1}{2} \mathrm{le}_\mathrm{eff} \, \gamma_2, \tag{31}$$

where the "effective" reduced Lewis number is

$$\mathrm{le}_\mathrm{eff} = \mathrm{le}_D + (\mathrm{le}_E - \mathrm{le}_D) \frac{b \, \mathcal{G}(a, b-1;\, \varphi)}{\mathcal{G}(a, b;\, \varphi)}. \tag{32}$$

With the mass flux m_1 determined, the normal velocity ahead of the flame, and hence the correction to the flame speed, can now be deduced. As $\eta \to -\infty$, $J - I = (\sigma - 1)/\sigma \gamma_1$ so that

$$m_1 \sim f_1 - \frac{\sigma - 1}{\sigma m_0} \gamma_1 \mathbb{K} - \frac{1}{m_0} I(\eta) \mathbb{K}_s$$

in this limit, and matching yields

$$V_{n_1}\big|_{n=0^-} - V_{f_1} = f_1 - \frac{\sigma - 1}{\sigma m_0} \gamma_1 \mathbb{K}, \quad \left. \frac{\partial V_{n_0}}{\partial n} \right|_{n=0^-} = -\mathbb{K}_s.$$

On the burned side of the flame, i.e., as $\eta \to +\infty$, we find that

$$m_1 \sim \lambda_\mathrm{b} (m_0 \kappa - \sigma^{-1} \mathbb{K}) \, \eta$$

and matching yields

$$V_{n_1}\big|_{n=0^+} - V_{f_1} = \sigma f_1, \quad \left. \frac{\partial V_{n_0}}{\partial n} \right|_{n=0^+} = -\mathbb{K} + \sigma m_0 \kappa.$$

These, in turn, can be expressed as jump relations across the whole flame as

$$[\![V_{n_1}]\!] = (\sigma-1)f_1 + \frac{\sigma-1}{\sigma m_0}\gamma_1\mathbb{K}, \quad \left[\!\!\left[\frac{\partial V_{n_0}}{\partial n}\right]\!\!\right] = (\sigma-1)m_0\kappa. \tag{33}$$

Finally, we note that the jump in the velocity gradient can be also deduced directly from the $\mathcal{O}(1)$ momentum equations; the consistency with the matching relations serve just as a verification of the calculation.

It is a straightforward, but tedious, matter to write the solution for the pressure and the tangential velocity components in the flame zone, which determine the jump in these variables across the flame. Since the relevant equations do not involve any additional effect associated with the heat-loss term, the results are similar to the adiabatic case analyzed in [8]. We will therefore avoid writing the details and just summarize the results in the next section. The detailed calculations involve the additional coefficients

$$\Gamma = (\sigma-1)\gamma_1 - (2\,\mathrm{Pr}-1)\gamma_3 + 2\,\mathrm{Pr}(\sigma-1)\lambda_\mathrm{b}, \quad \gamma_3 = \int_1^\sigma \lambda(x)\,\mathrm{d}x,$$

which are presented here for completeness.

6 The hydrodynamic model

The multi-scale approach of the preceding sections has reduced the full set of governing equations to the following simplified model. On either side of the flame sheet the flow field, to $\mathcal{O}(\delta)$, is described by

$$\boldsymbol{\nabla}\cdot\mathbf{v} = 0, \tag{34}$$

$$\rho\frac{\mathrm{D}\mathbf{v}}{\mathrm{D}t} = -\boldsymbol{\nabla}p + \delta\,\mathrm{Pr}\;\boldsymbol{\nabla}\cdot\lambda\left(\boldsymbol{\nabla}\mathbf{v} + (\boldsymbol{\nabla}\mathbf{v})^\mathrm{T}\right) \tag{35}$$

with the density and viscosity piecewise constant functions, given by

$$\rho = \begin{cases} 1 \\ 1/\sigma \end{cases}, \quad \lambda = \begin{cases} 1 & F<0 \\ \lambda_\mathrm{b} & F>0. \end{cases}$$

The jump in pressure and velocities across the flame are given by

$$[\![\rho(\mathbf{v}\cdot\mathbf{n} - V_f)]\!] = \frac{\delta}{m_0}\,\frac{\sigma-1}{\sigma}\,\gamma_1\mathbb{K} \tag{36}$$

$$[\![\mathbf{n}\times(\mathbf{v}\times\mathbf{n})]\!] = \frac{\delta}{m_0}\,\{-(\lambda_\mathrm{b}\,\mathrm{Pr}+\gamma_1)\,[\![\mathbf{n}\times(\nabla\times\,\mathbf{v})]\!] + 2\,\mathrm{Pr}\,(\lambda_\mathrm{b}-1)\;(\mathbf{n}\times(\mathbf{E}\cdot\mathbf{n})\times\mathbf{n})\}, \tag{37}$$

$$[\![p+\rho(\mathbf{v}\cdot\mathbf{n})(\mathbf{v}\cdot\mathbf{n}-V_f)]\!] = \frac{\delta}{m_0}\left\{\gamma_1\,[\![\mathbf{n}\cdot\nabla p]\!] + \frac{\sigma-1}{\sigma}\gamma_1 V_f\,\mathbb{K} + \Gamma\,\kappa + 2\,\mathrm{Pr}(\lambda_\mathrm{b}-1)\,(\mathbf{n}\cdot\mathbf{E}\cdot\mathbf{n})\right\}, \tag{38}$$

with the right-hand side evaluated at $n = 0^-$. An equation for the flame speed, correct to $\mathcal{O}(\delta)$, may be written in the form

$$S_f^2\log S_f^2 = -q_\mathrm{L} - 2\delta\left\{\left(\alpha S_f - \frac{k\gamma_c}{S_f}\right)\kappa + \left(\alpha - \frac{k\gamma_s}{S_f^2}\right)\mathbb{K}_s\right\}, \tag{39}$$

where $q_\mathrm{L} \equiv k(q_\mathrm{u}+q_\mathrm{b})$ is the total heat loss from the unburned and burned sides, and

$$\gamma_s = \frac{q_\mathrm{b}}{2\sigma}\left((2\sigma-1)\gamma_1 - \lambda_\mathrm{b}\right) + \frac{\sigma-1}{\sigma}\gamma_1 q_\mathrm{u} + s_2, \quad \gamma_c = \frac{2\sigma-1}{2\sigma}q_\mathrm{b}(\gamma_1+\lambda_\mathrm{b}) + \frac{\sigma-1}{\sigma}\gamma_1 q_\mathrm{u} - s_4,$$

$$s_4 = s_1 - s_2 + s_3 = \int_1^\sigma\left(\int_y^\sigma \frac{\lambda(x)}{x}\mathrm{d}x - \lambda(y)\right)\left(\int_y^\sigma \frac{\lambda(x)g(x)}{(x-1)^2}\mathrm{d}x\right)\mathrm{d}y.$$

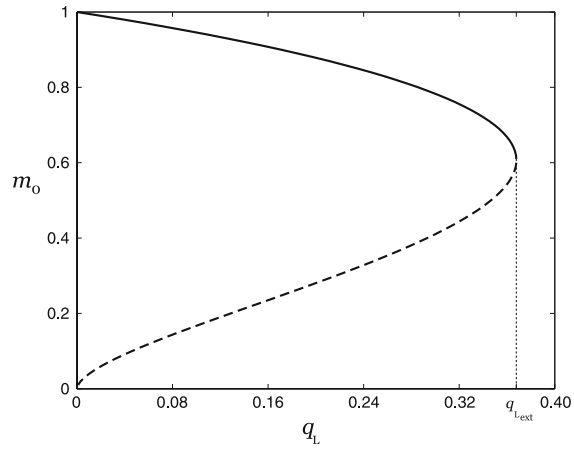

Fig. 1 The (dimensionless) flame speed, or mass burning rate, of a planar flame as a function of the total heat loss q_L. The dashed branch, along which the speed increases with increasing q_L correspond to unstable states that cannot be realized physically. The turning point thus corresponds to extinction

Since

$$S_f \equiv \left.\frac{\mathbf{v}\cdot\nabla F}{|\nabla F|}\right|_{n=0^-} - \frac{1}{|\nabla F|}\frac{\partial F}{\partial t}, \tag{40}$$

Eq. (39) can equivalently be thought as determining the flame-front position.

Equations (34–39), when supplemented with initial and boundary conditions, constitutes a nonlinear free-boundary problem for the pressure, $p(\mathbf{x}, t)$, the velocity, $\mathbf{v}(\mathbf{x}, t)$, and the instantaneous shape and position of the flame-front interface $F(\mathbf{x}, t)$. All the combustion influences are accounted for in the flame-speed equation that determines how the front evolves. The model is therefore appropriately referred to as a *hydrodynamic model*. It is easy to verify that, in the absence of heat loss, the formulation reduces to that presented earlier in [8]. Versions of the adiabatic model have been successfully used in analytical studies aimed, for example, at examining the nature of the flow induced by thermal expansion [20] and the stability of planar [4–6] and spherically expanding [17] flames, and in numerical studies aimed at simulating the nonlinear development of large-scale flames [21].

To leading order, the flame speed of a curved flame based on (39) is a constant equals to the speed of a planar flame experiencing the same losses. The dependence of the planar non-adiabatic flame speed on the total loss is shown in Fig 1. For a given q_L there are two possible solutions, provided $q_L < e^{-1}$, and no solution for $q_L > e^{-1} \equiv q_{ext}$; note that $q_{ext} = 0.3678$ which means that, approximately, the losses should not exceed 37% of the heat generated. The states on the lower branch (dashed curve), corresponding to a flame speed that increases with increasing q_L, are unstable and, therefore, cannot be realized physically. Possible stable states would correspond to the upper branch (solid curve). When increasing q_L, starting with the adiabatic laminar flame speed ($m_0 = 1$), the speed decreases until extinction occurs at $q_L = q_{ext}$. The flame speed at extinction $m_0 = \sqrt{e}$ is approximately 61% of the laminar flame speed S_L.

Effects of curvature and strain are determined through the $\mathcal{O}(\delta)$ terms in the equation. For adiabatic flames strain and curvature combine into a single quantity, flame stretch $\mathbb{K}$, and the flame speed is found to vary linearly with stretch. The proportionality constant α, which is the only mixture-sensitive parameter in the model, is known as the Markstein number (or Markstein length when multiplied in dimensional form). It depends on the effective Lewis number of the mixture,

$$\mathrm{Le}_{\mathrm{eff}} = \frac{\mathrm{Le}_E + \mathrm{Le}_D\mathcal{A}}{1+\mathcal{A}}, \quad \mathcal{A} \equiv \frac{\mathcal{G}(a,b;\varphi)}{b\,\mathcal{G}(a,b-1;\varphi)} - 1,$$

a weighted average of the separate Lewis numbers associated with the two reactants (see Eq. 32). Note that for conditions remote from stoichiometry, corresponding to a large value of φ, the effective Lewis number is that of the deficient reactant, that is, the fuel in a lean mixture and the oxidizer in a rich one. For non-adiabatic flames the individual influence of strain and curvature on the flame speed may be quite different. It is convenient in this case to re-scale the flame speed using m_0, rather than the planar adiabatic value, as reference with the newly scaled

quantity denoted by $\hat{S}_f = S_f/m_0$. The diffusion length, or flame thickness, must also be modified, which requires replacing δ by $\hat{\delta} = \delta/m_0$. Then the flame-speed equation (39) simplifies to

$$\hat{S}_f = 1 - \hat{\delta}(\alpha_c \kappa + \alpha_s \mathbb{K}_s), \tag{41}$$

where

$$\alpha_s = \frac{m_0^2\alpha - k\gamma_s}{m_0^2 - q_{\mathrm{L}}}, \quad \alpha_c = \frac{m_0^2\alpha - k\gamma_c}{m_0^2 - q_{\mathrm{L}|}}.$$

The dependence on curvature and strain is again linear but there are two distinct Markstein numbers, one associated with strain, α_s, and the other with curvature, α_c. They become equal (i.e. , $\alpha_s = \alpha_c = \alpha$) only when $q_{\mathrm{L}} = 0$. As a final point we note that the conditions leading to extinction may now be modified slightly so that $q_{\mathrm{ext}} = \mathrm{e}^{-1} + \delta\varepsilon$ with ε depending on time and location. Although one can write an explicit expression for ε, the general result is not particularly instructive. The discussion is left to specific applications, such as the stabilization of Bunsen flames presented below.

It can be easily verified that when velocities are rescaled with respect to m_0 and pressure with respect to m_0^2, the governing equations (34–35) and jump relations (36–38) become identical to the similar relations for the adiabatic model [8] after replacing δ by $\hat{\delta}$. Hence, when the planar *non-adiabatic* flame speed rather than S_{L} is used as reference, the only difference in the mathematical formulation when including heat losses is the propagation speed that must now obey Eq. 41 with the two distinct Markstein numbers.

The accurate determination of Markstein numbers for various mixtures has been the subject of extensive studies, prompted primarily by the theoretical predictions. Overall, the theoretical predictions were found to correlate well with the experimental record. These studies, however, have focused on adiabatic flames and the objective here is to assess the effect of heat loss. Figure 2 shows the dependency of the Markstein coefficients on equivalence ratio for selected fuel/air mixtures with $a = b = 1$ and the three values of q_{L}. For these calculations, the realistic choices $\lambda \sim T^{1/2}$ and $g = T^4 - 1$ have been made. The magnitude of the Markstein numbers increases significantly with increasing q_{L} and at near-extinction conditions it may be larger by nearly a factor of five. For relatively small losses, the difference between α_s and α_c is small but it is accentuated as q_{L} approaches its extinction value; in this limit curvature has a more pronounced influence than strain on the flame speed. A methane–air mixture appears to be exceptional; the diffusivities of the fuel and oxidizer for this mixture are nearly equal. Since for off-stoichiometric mixtures the diffusivity of the deficient reactant is the controlling factor, there are significant differences between the various mixtures for lean conditions. The Markstein numbers of the heavier fuels are much larger and then tend to decrease with increasing mixture strength. The Markstein numbers of light fuels are much smaller and they tend to increase with increasing mixture strength. For rich conditions, all the mixtures tend to approximately the same limiting value, because it is the diffusivity of the oxidizer which is the controlling factor; the small difference that remain are due to variations in the thermal expansion parameter σ. Note also that for lean conditions, the Markstein number of lighter fuels, such as hydrogen, may become negative as the losses become significantly large. This implies that unlike hydrocarbon mixtures, for which the flame speed decreases when the flame is positively stretched, the flame speed of a hydrogen–air mixture may increase when it is stretched.

Figure 3 shows the dependence of the Markstein numbers on the heat-loss parameter q_{L} for selected values of the effective reduced Lewis number $\mathrm{Le}_{\mathrm{eff}}$. For small and moderate losses, a very little difference is seen between the values of α_s and α_c. However, when extinction conditions are approached, the deviation become significant. It should be noted that the graphs in this figure do not correspond to a particular mixture, as in Fig. 2, but rather to a mixture of a given strength. For example, the curve with negative $\mathrm{Le}_{\mathrm{eff}}$ may be associated with a lean hydrogen–air mixture for which both α_s and α_c decrease as the losses increase. The curve with positive $\mathrm{Le}_{\mathrm{eff}}$ may be associated with a lean hydrocarbon–air mixture (except for methane) for which both α_s and α_c increase as the losses increase. The curve with $\mathrm{Le}_{\mathrm{eff}} = 0$ may be associated with a lean methane–air mixture for which α_s decreases with increasing q_{L} while α_c increases.

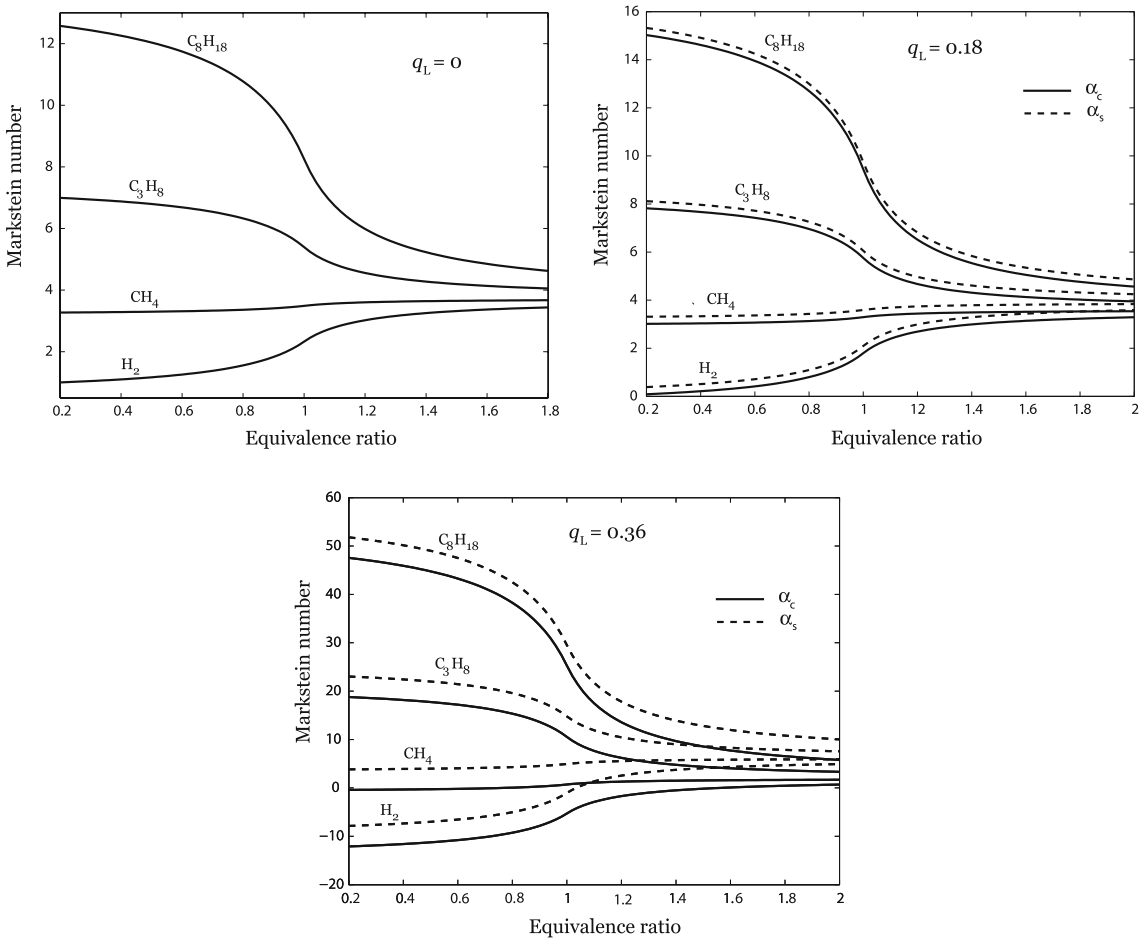

Fig. 2 The Markstein numbers α_s and α_c associated with strain and curvature, respectively, as a function of equivalence ratio for three selected values of heat loss $q_L = 0, 0.18, 0.36$ (for the adiabatic case $q_L = 0$ the values $\alpha_s = \alpha_c = \alpha$. Note also, for reference purpose, that $q_{ext} = 0.3678$

7 Bunsen-burner flame

With the exception of few simple configurations a complete solution of the hydrodynamic model requires a non-trivial numerical scheme [22]. Nevertheless, when the flow field of the incoming fresh mixture is known, some conclusions can be made about the flame speed and shape. Here we shall investigate the extinction characteristics of a stationary Bunsen burner flame under non-adiabatic conditions, assuming that the flow issuing from the burner is a Poiseuille flow.

We consider a slot burner of width $2L$ and thus restrict attention to two dimensions (x, y). Since the burner width, typically a few centimeters, is large compared to the flame thickness (a fraction of a millimeter), the flame can be properly treated as a hydrodynamic discontinuity. The flow of the mixture issuing from the burner is unidirectional with (dimensionless) velocity $u(y) = U(1 - y^2)$, where the centerline velocity U is measured in units of the (adiabatic) laminar flame speed. The flame front may be expressed in the form $F(x, y) \equiv x - f(y) = 0$, so that unit vectors normal and tangential to the flame front are given by

$$\mathbf{n} = \frac{\mathbf{i} - f_y \mathbf{j}}{(1 + f_y^2)^{1/2}}, \quad \mathbf{e} = \frac{f_y \mathbf{i} + \mathbf{j}}{(1 + f_y^2)^{1/2}},$$

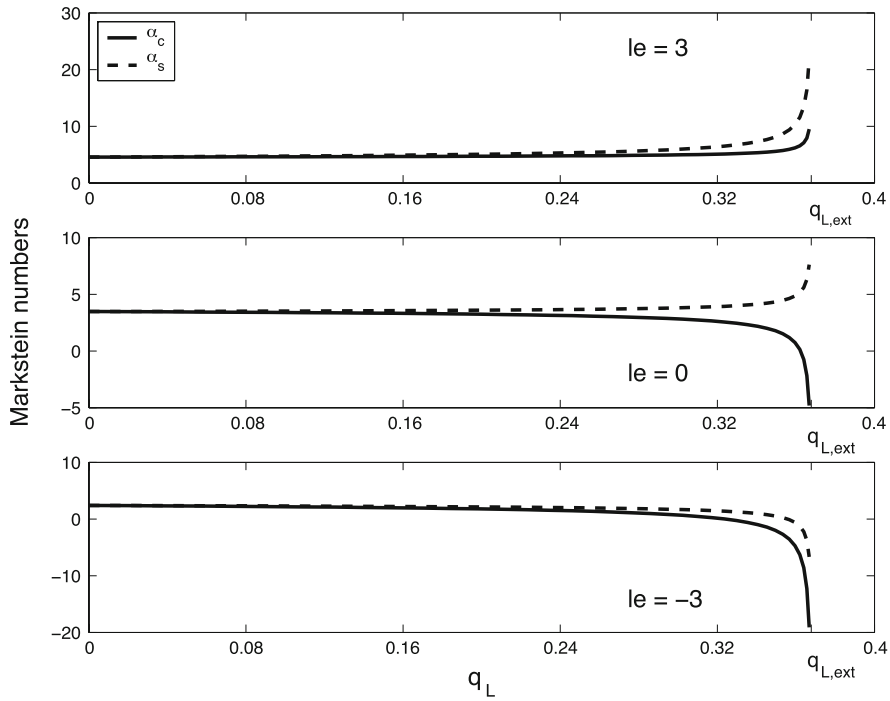

Fig. 3 The dependence of the Markstein numbers associated with strain and curvature, α_s and α_c respectively, on heat loss for selected value of the reduced Lewis number

with **i**, **j** unit vectors in the x and y directions, respectively. Subscript y denotes here partial differentiation. Assuming a symmetrical shape with respect to the axis $y = 0$, the relations (39)–(40) yield, to leading order, an expression for the slopes,

$$f_y = \pm\frac{1}{m_0}\sqrt{U^2(1-y^2)^2 - 1},$$

with m_0 determined from the relation $m_0^2 \log m_0^2 = -q_{\mathrm{L}}$. This equation can be integrated to determine the flame shape $x = f(y)$. Note that a stationary flame is restricted to the interval $|y| < ((U - m_0)/U)^{1/2}$; the flame cannot be stabilized against the flow at locations where the local gas velocity is lower than m_0. The flame spreads out further in the presence of heat loss because the speed of the non-adiabatic flame is lower. With $f(y)$ known, the curvature and strain rate may be computed from $\kappa = f_{yy}(1 + f_y^2)^{-3/2}$ and $\mathbb{K}_s = f_y u_y/(1 + f_y^2)$. The $\mathcal{O}(\delta)$ correction to the speed m_0 is computed from

$$S_f^2 \log S_f^2 = -q_{\mathrm{L}} - \frac{2\delta u_y S_f}{(u^2 - S_f^2)^{1/2}}\left(\alpha - k\gamma_c\frac{1}{u^2} - k\gamma_s\frac{u^2 - S_f^2}{u^2 S_f^2}\right), \tag{42}$$

from which the corresponding adjustment in flame shape is obtained.

The preceding perturbation scheme fails near the tip because of the discontinuity in slopes exhibited already in the leading term. The resolution requires a complete hydrodynamic description which is outside the scope of this paper. Insight into the nature of the solution, however, can be obtained if one adopts the $\mathcal{O}(\delta)$ equation for the flame speed (42) as an approximation. This is easily done numerically leading to the profiles shown in Fig. 4. The profiles are plotted for several values of q_{L}, with a sufficiently small $\delta = 0.01$. It is seen that the flame height increases and its base spreads out as the losses increase. Further refinement of the solution curves near the centerline demonstrates that the flame tips are indeed rounded. We recall that flame extinction would first occur when q_{L} exceeds the value $\mathrm{e}^{-1} + \delta\varepsilon$, with ε depending on the location. In the figure this occurs near the tip for the largest value of q_{L}. The flame speed as a result of heat losses is small enough and cannot be balanced by the relatively high velocity of

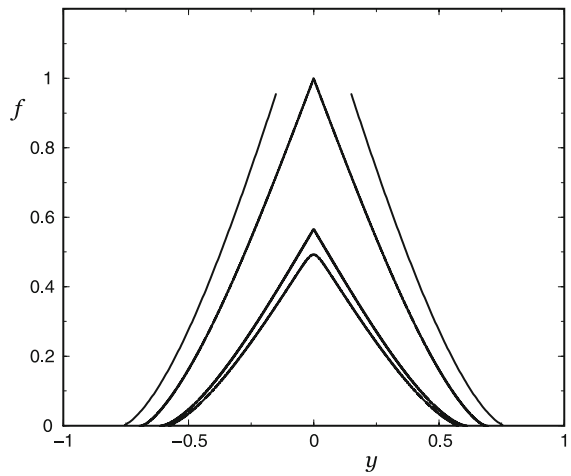

Fig. 4 Profiles of Bunsen (slot) burner flames for increasing values of the heat-loss parameter $q_L = 0,\ 0.25e^{-1}, 0.5e^{-1}, e^{-1}+0.01$. The flame height increases and its base spreads out when increasing the level of heat loss, with tip opening occurring at near-extinction conditions. The profiles are calculated for $\delta = 0.01, \alpha = 1$ and $\sigma = 6$

the upcoming gas near the centerline. Consequently the flame gets blown-off locally leading to a tip opening. Tip opening has been observed in Bunsen flames [23, Sect. V.3, 24] and could result from heat losses, as suggested here, as well as from an imbalance in diffusion rates as discussed in [25].

8 Conclusions

We have presented a multi-scale analysis of premixed flame propagation that incorporates the effects of volumetric heat loss. By examining the problem on separate length scales, we have demonstrated that the mathematical problem reduces to a free-boundary problem with the flame represented by a surface of density discontinuity advected and distorted by the large-scale flow. By analyzing the flame structure, which evolves on the much shorter diffusive length scale, we derived jump relations for the flow variables across the flame surface, as well as an explicit relation for the propagation speed of the moving front. Hydrodynamic theories of adiabatic premixed flames have been derived previously that allow for quite general conditions, including variable transport, effects of stoichiometry and arbitrary reaction orders. In the present theory, we have extended those models to include volumetric heat loss, such as radiative loss, which are unavoidable in most flame systems, and are known to significantly affect flame dynamics, including extinction.

The interpretation of the results of the present theory has yielded the following conclusion. When the planar non-adiabatic flame speed is used as the reference velocity, our model can be expressed in a form that is nearly identical to the adiabatic model. Specifically, the jump conditions across the flame front take similar forms with the only difference arising in the flame-speed equation which exhibits a dependence on flame curvature and hydrodynamic strain, but with two distinct coefficients, or Markstein numbers. These parameters depend now on the integrated heat loss across the whole flame. To illustrate these effects we have assessed the dependence of the Markstein numbers on equivalence ratio as conditions approach the flammability limit. Finally, as an illustration we employed our model to study the quenching characteristics of a Bunsen-burner flame subject to radiative heat loss. We have shown that these losses may be also responsible for the observed phenomenon of tip opening in Bunsen flames in addition to differential diffusion effects that have been known as responsible for this phenomenon.

Results of the present theory may be exploited in future research activities to complement earlier works on adiabatic flames. Our theory provides an explicit dependence of fundamental flame parameters on volumetric losses, as well as variable mixture strength, arbitrary reaction order, and realistic transport coefficients, and thus it mimics a wide range of actual experimental conditions. The explicit expressions derived here for burning rate, Markstein numbers, etc. may be used by experimentalists to correlate data from flame measurements. The general formulation presented here can also be used in numerical simulations of turbulent premixed flames, particularly in the lami-

nar flamelet regime, where heat losses may affect the dynamics of the individual flamelets and consequently the behavior of the overall flame brush.

The multi-scale methodology presented here can be extended to study the dynamics of flames in heterogeneous media, such as liquid-fuel sprays or dusty gases. In such problems there is a condensed phase in the form of liquid droplets or solid particles dispersed in a gas phase. Viewed on the large hydrodynamic scale, the flame appears separating the unburnt mixture from the burnt products, but the details within the flame zone are far more complex than in single-phase combustion. On the smaller scale one must account for mass, momentum and energy interactions between the gaseous and condensed phases as well as for the specific properties of the condensed phase such as particle size, fuel volatility, and thermodynamic properties. The mathematical analysis of two-phase combusting flows has not received the proper attention it deserves and the proposed work provides a conceptual framework for broadening our fundamental understanding of these practical flow systems.

Acknowledgements This work has been supported by the National Science Foundation under grant CBET-0733146. MM also acknowledges support of the US-Israel Bi-National Science Foundation.

Appendix: Nomenclature

$\mathcal{B}$	Pre-exponential factor in the expression for the reaction rate
c_p	Specific heat of the mixture
D_i	Molecular (binary) diffusivity of species i
$\mathcal{D}_{th}$	Thermal diffusivity of the mixture
E_a	Activation energy
F	Function identifying the lame surface
h_i	Enthalpy function associated with species i
$\mathbb{K}$	Flame stretch
$\mathbb{K}_s$	Local strain rate at the flame surface
le	Reduced Lewis number
l_p	Planck mean absorption length
L	Hydrodynamic length scale
L_D	Diffusion length scale
Le	Lewis number
$\mathcal{M}$	Chemical symbol
n	Coordinate in a normal direction to the flame surface
p	Pressure
Pr	Prandtl number
q_i	Integrated heat losses in burned and unburned regions
q_L	Total heat losses
Q	Total heat release
Q_L	Heat loss per unit volume per unit time
R^o	Universal gas constant
S_L	Flame speed
T	Temperature
T_a	Adiabatic flame temperature
v, V	Velocity
W_i	Molecular weight of species i
Y_i	Mass fraction of species i

Greek symbols

α	Markstein number
β	Zel'dovich number
γ_i	Constants depending only on σ
δ	Ratio of lengths L_D/L
η	Stretched normal coordinate
θ, Θ	Non-dimensional temperatures
κ	Local curvature of the flame surface
λ	Thermal conductivity
μ	Viscosity
ν_i	Stoichiometric coefficient of species i
ϖ	Reaction rate
ρ	Density
σ	Thermal expansion parameter
Φ	Ratio of mass of excess to deficient reactants
φ	Measure of departure from stoichiometry; defined by $\beta(\Phi - 1)$

Subscripts

b	Burned
D	Deficient
E	Excess
u	Unburned

Superscripts

T	Transpose
$*$	Quantity evaluated on burned side of reaction zone

References

1. Darrieus G (1938) Propagation d'un front de flamme. Unpublished work; presented at La Technique Moderne (Paris) and in 1945 at Congrès de Mécanique Appliquée (Paris)
2. Landau L (1944) On the theory of slow combustion. Acta Physicochimica URSS 19:77–85
3. Markstein GH (1964) Nonsteady flame propagation. Pergamon
4. Pelce P, Clavin C (1982) Influence of hydrodynamics and diffusion upon the stability limits of laminar premixed flames. J Fluid Mech 124:219–237
5. Matalon M, Matkowsky BJ (1982) Flames as gasdynamic discontinuities. J Fluid Mech 124:239–259
6. Frankel M, Sivashinsky GI (1982) The effect of viscosity on hydrodynamic stability of plane flame front. Combust Sci Tech 29:207–224
7. Keller D, Peters N (1994) Transient pressure effects in the evolution equation for premixed flame fronts. Theor Comput Fluid Dyn 6:141–159
8. Matalon M, Cui C, Bechtold JK (2003) Hydrodynamic theory of premixed flames: effects of Stoichiometry, variable transport coefficients and reaction orders. J Fluid Mech 487:179–210
9. Class AG, Matkowsky BJ, Klimenko AY (2003) A unified model of flames as gasdynamic discontinuities. J Fluid Mech 491: 11–49
10. Zeldovich YaB, Barenblatt GI, Librovich VB, Mahkviladze GM (1985) The mathematical theory of combustion and explosions. Consultants Bureau, New York
11. Joulin G, Clavin C (1976) Asymptotic analysis of the conditions of laminar flame extinction. Acta Astronaut 3:223–240
12. Buckmaster JD (1976) The quenching of deflagration waves. Combust Flame 26:151–162
13. Williams FA (1985) Combustion Theory, 2nd edn. Addison-Wesley, CA
14. Clavin P, Nicoli C (1985) Effect of heat losses on the limits of stability of premixed flames propagating downwards. Combust Flame 60:1–14
15. Bechtold JK, Cui C, Matalon M (2004) The role of radiative losses in self-extinguishing and self-wrinkling flames. Proc Combust Inst 30:177–184
16. Buckmaster JD, Ludford GSS (1982) Theory of laminar flames. Cambridge University Press
17. Bechtold JK, Matalon M (1999) Effects of stoichiometry on stretched premixed flames. Combust Flame 119:217–232
18. Antoniou ES, Bechtold JK, Matalon M (2004) A diffusional-thermal theory of near-stoichiometric premixed flames. SIAM J Appl Math 64:1434–1456
19. Matalon M (1983) On flame stretch. Combust Sci Technol 31:169–181
20. Eteng E, Ludford GSS, Matalon M (1986) Displacement effects of a flame in a stagnation-point flow. Phys Fluid 29(7):2172–2180
21. Rastigeyev Y, Matalon M (2006) Nonlinear evolution of hydrodynamically unstable premixed flames. J Fluid Mech 554:371–392
22. Rastigeyev Y, Matalon M (2006) Numerical simulations of flames as gasdynamic discontinuities. Combust Theory Model 10(3):459–481
23. Lewis B, von Elbe G (1987) Combustion, flames and explosions of gases, 3rd edn. Academic Press
24. Mizomoto M, Asaka Y, Ikai S, Law CK (1984) Effects of preferential diffusion on the burning intensity of curved flames. Proc Combust Inst 20:1933–1939
25. Cui C, Matalon M, Daou J, Dold J (2004) Effects of differential diffusion on thin and thick flames propagating in channels. Combust Theory Model 8:41–64